47th AIAA Aerospace Sciences Meeting Including The New Horizons Forum and Aerospace Exposition
5 - 8 January 2009, Orlando, Florida

AIAA 2009-240

DNS of auto–ignition in turbulent diffusion H_2/air flames

Jeff Doom* and Krishnan Mahesh†

University of Minnesota, Minneapolis, MN, 55455, USA

Direct numerical simulation (DNS) is used to study auto–ignition of turbulent diffusion flames. A novel, all–Mach number algorithm developed by Doom et al[1] is used. The chemical mechanism is a nine species, nineteen reaction mechanism for H_2 and Air from Mueller at el.[2] Simulations of three dimensional turbulent diffusion flames are performed. Isotropic turbulence is superimposed on an unstrained diffusion flame where diluted H_2 at ambient temperature interacts with hot air. Both, unity and non–unity Lewis number are studied. The results are contrasted to the homogeneous mixture problem and laminar diffusion flames. Results show that auto–ignition occurs in fuel lean, low vorticity, high temperature regions with low scalar dissipation around a most reactive mixture fraction, ζ_{MR} (Mastorakos et al.[3]). However, unlike the laminar flame where auto-ignition occurs at ζ_{MR}, the turbulent flame auto–ignites over a very broad range of ζ around ζ_{MR}, which cannot completely predict the onset of ignition. The simulations also study the effects of three-dimensionality. Past two–dimensional simulations (Mastorakos et al.[3]) show that when flame fronts collide, extinction occurs. However, our three dimensional results show that when flame fronts collide; they can either increase in intensity, combine without any appreciable change in intensity or extinguish. This behavior is due to the three–dimensionality of the flow.

I. Introduction

The auto–ignition of turbulent diffusion flames is central to applications such as diesel engines and scramjet engines where fuel is injected into hot oxidizer. Fuel and oxidizer mix through convection and diffusion, then auto–ignite due to the high temperatures of the oxidizer. Direct numerical simulation (DNS) is used to study a diffusion flame where fuel (hydrogen/nitrogen) reacts with air (oxygen/nitrogen). For laminar flames, fuel and oxidizer diffuse, then react, yielding products. In turbulent flames, one might see auto–ignition, extinction and even re–ignition due to the turbulence.

Mahalingam et al.[4] performed DNS of three-dimensional turbulent non–premixed flames with finite rate chemistry. They incorporated one–step and two–step reaction models for the chemistry. Their results show that the intermediate species concentration overshoots the experiments. They suggest that this behavior is due to time–dependent strain rates in the turbulent flow. Montgomery et al.[5] also performed DNS of a three-dimensional turbulent hydrogen–oxygen non–premixed flame using a reduced mechanism (7–species, ten–reactions). The simulations were used to suggest a mixture fraction and progress variable model for the chemical reactions. Im et al.[6] performed DNS of two–dimensional turbulent non–premixed hydrogen–air flames to study auto–ignition. They show that peak values of HO_2 align with maximum scalar dissipation during ignition. Im et al. also noted that weak and moderate turbulence enhanced auto–ignition while stronger turbulence delayed ignition. Echekki & Chen[7] used DNS to study auto–ignition of a hydrogen/air mixture in

*Graduate Research Assistant
†Associate Professor

two dimensional turbulence. Their results show spatially localized sites where auto–ignition begins, which they define as a "kernel". These kernels have a build up of radicals at high temperatures, fuel–lean mixtures, and low dissipation rates. Mastorakos et al. performed two–dimensional simulation of auto–ignition of laminar and turbulent diffusion flames with one–step chemistry. They found that ignition always occurs at a well–defined mixture fraction (ζ_{MR}). Hilbert & Thevenin[8] performed similar simulations to Mastorakos et al.[3] and Im et al.[6] The difference between Hilbert & Thevenin[9] and others is that the simulation uses multicomponent diffusion velocities.

A significant difference between the past work cited above, and our DNS is that we perform fully three dimensional simulations using finite rate chemistry. Also, we incorporate the Mueller mechanism for hydrogen/air (nine species and nineteen reaction) and not a reduced mechanism. The objectives of our simulations are: (i) to study major differences between two dimensional and three dimensional simulations of turbulent diffusion flames. In particular, what happens to the flame front in three dimensions? (ii) How do the ignition kernels evolve in time? (iii) What is the effect of unity Lewis number and non–unity Lewis number on ignition, and (iv) How does the mixture fraction compare to a passive scalar?

This paper is organized as follows. The governing equations and numerical method are described in section II and section II.A. Section III provides details of the laminar diffusion flame, turbulent diffusion flame and validation. The simulations results are discussed in section IV. In the results section, the homogeneous problem (IV.A), auto–ignition (IV.B), Lewis number (IV.C) and flame front evolution (IV.D) are discussed in detail. A brief summary in section V concludes the paper.

II. Governing equations

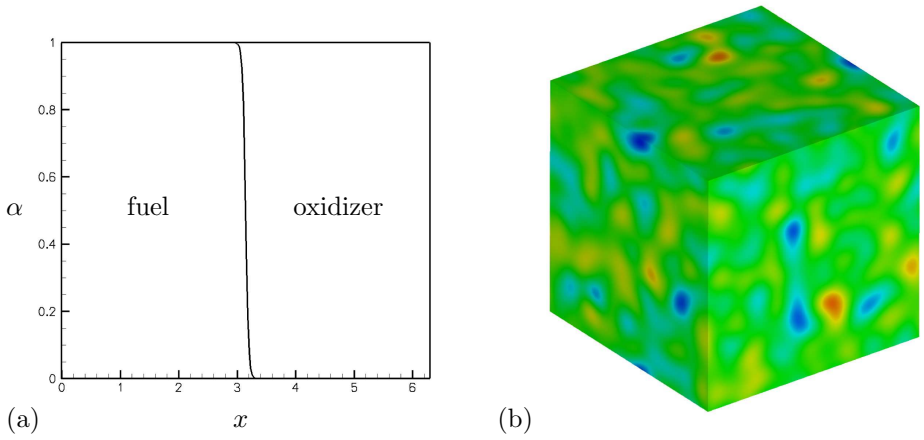

Figure 1. Schematic of initial conditions for the turbulent diffusion flame. (a) Diffusion flame and (b) Isotropic turbulence.

The governing equations are the unsteady, compressible, reacting Navier–Stokes equations:

$$\frac{\partial \rho^d}{\partial t^d} + \frac{\partial \rho u_j^d}{\partial x_j^d} = 0, \tag{1}$$

$$\frac{\partial \rho^d Y_k^d}{\partial t^d} + \frac{\partial \rho Y_k^d u_j^d}{\partial x_j^d} = \frac{\partial}{\partial x_j^d}\left(\rho^d D_k^d \frac{\partial Y_k^d}{\partial x_j^d}\right) + \dot{\omega}_k^d, \tag{2}$$

$$\frac{\partial \rho^d u_i^d}{\partial t^d} + \frac{\partial \rho^d u_i^d u_j^d}{\partial x_j^d} = -\frac{\partial p^d}{\partial x_i^d} + \frac{\partial \tau_{ij}^d}{\partial x_j^d} \tag{3}$$

$$\frac{\partial \rho^d E^d}{\partial t^d} + \frac{\partial \left(\rho^d E^d + p^d\right) u_j^d}{\partial x_j^d}$$
$$= \frac{\partial \tau_{ij}^d u_i^d}{\partial x_j^d} + \frac{\partial}{\partial x_j^d}\left(\mu^d \frac{c_p^d}{Pr}\frac{\partial T^d}{\partial x_j^d}\right) + \sum_{k=1}^{N} Q_k^d \dot{\omega}_k^d, \tag{4}$$
$$p^d = \rho^d R^d T^d = \rho^d \frac{R_u}{W^d} T^d. \tag{5}$$

The superscript 'd' denotes the dimensional value. From Doom et al.,[1] non–dimensional variables are defined as:

$$\rho = \frac{\rho^d}{\rho_r}, \quad u_i = \frac{u_i^d}{u_r}, \quad t = \frac{t^d}{L/u_r}, \quad \mu = \frac{\mu^d}{\mu_r}, \quad p = \frac{p^d - p_r}{\rho_r {u_r}^2}, \tag{6}$$
$$T = \frac{T^d}{T_r}, \quad M_r = \frac{u_r}{a_r} = \frac{u_r}{\sqrt{\gamma R_r T_r}}, \quad p_r = \rho_r R_r T_r, \tag{7}$$
$$Y_k = \frac{Y_k^d}{Y_r}, \quad D_k = \frac{D_k^d}{u_r L}, \quad \dot{\omega}_k = \frac{L\dot{\omega}_k^d}{u_r \rho_r Y_r}, \quad Q_k = \frac{Y_r Q_k^d}{c_{p,r} T_r}, \tag{8}$$
$$R_r = \frac{R_u}{W_r}, \quad Le_k = \frac{Sc_k}{Pr} \quad , \quad \text{and} \quad W = \frac{W^d}{W_r}. \tag{9}$$

Let the subscript 'r' denote the reference variable. Note that pressure is non–dimensionalized using an incompressible scaling motivated by Thompson.[10] Therefore, the non–dimensional governing equations are:[1]

$$\frac{\partial \rho}{\partial t} + \frac{\partial \rho u_j}{\partial x_j} = 0, \tag{10}$$
$$\frac{\partial \rho Y_k}{\partial t} + \frac{\partial \rho Y_k u_j}{\partial x_j} = \frac{1}{ReSc_k}\frac{\partial}{\partial x_j}\left(\mu \frac{\partial Y_k}{\partial x_j}\right) + \dot{\omega}_k, \tag{11}$$
$$\frac{\partial \rho u_i}{\partial t} + \frac{\partial \rho u_i u_j}{\partial x_j} = -\frac{\partial p}{\partial x_i} + \frac{1}{Re}\frac{\partial \tau_{ij}}{\partial x_j}, \tag{12}$$
$$M_r^2\left[\frac{\partial}{\partial t}\left(p + \frac{\gamma-1}{2}\rho u_i u_i\right) + \frac{\partial}{\partial x_j}\left(\gamma p + \frac{\gamma-1}{2}\rho u_i u_i\right) u_j\right] + \frac{\partial u_j}{\partial x_j}$$
$$= \frac{(\gamma-1)M_r^2}{Re}\frac{\partial \tau_{ij} u_i}{\partial x_j} + \frac{1}{RePr}\frac{\partial}{\partial x_j}\left(\frac{\mu}{W}\frac{\partial T}{\partial x_j}\right) + \underbrace{\sum_{k=1}^{N} Q_k \dot{\omega}_k}_{\dot{\omega}_n}, \tag{13}$$
$$\frac{\rho T}{W} = \gamma M_r^2 p + 1. \tag{14}$$

Here, ρ, T, p, u_i and Y_k denote non–dimensional density, temperature, pressure, velocities and mass fraction of 'k' species respectively. The viscous stress tensor $\tau_{ij} = \mu\left(\frac{\partial u_i}{\partial x_j} + \frac{\partial u_j}{\partial x_i} - \frac{2}{3}\frac{\partial u_k}{\partial x_k}\delta_{ij}\right)$. The source term is denoted as: $\dot{\omega}_k$ which is modeled using the Arrhenius law. The heat of reaction per unit mass in the energy equation is Q_k and $\sum Q_k \dot{\omega}_k$ or $\dot{\omega}_n$ is the heat release due chemical reactions. Sc_k is the Schmidt number for the k^{th} species, Pr is the Prandtl number, and Re is the Reynolds number. W is the mean molecular weight of the mixture.

II.A. Numerical method

The numerical algorithm is discussed in detail by Doom et al.[1] The algorithm is fully implicit, spatially non–dissipative and second order in time & space. The thermodynamic variables and

species are staggered in time from velocity. All variables are co–located in space. A pressure–correction method is used to enforce velocity divergence obtained from the energy equation. The discrete equations discretely conserve kinetic energy in the incompressible, non–reacting, inviscid limit. These features make the algorithm stable and accurate at high Reynolds numbers, and efficient at both low and finite Mach numbers. These features are attractive for DNS of compressible turbulent reacting flows.

III. Problem statement

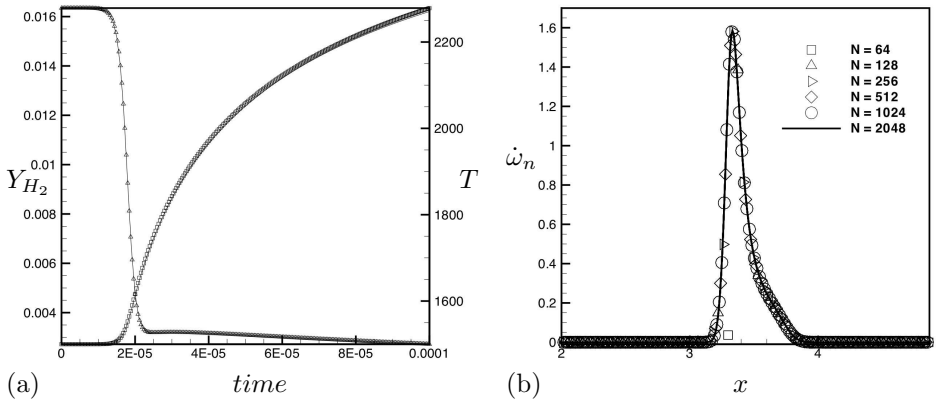

Figure 2. (a) Comparison of a major species & temperature between Chemkin and present algorithm for a well–stirred reactor. ($[Y_{H_2}]$ ——— Algorithm, △ Chemkin & $[T]$ – – – – Algorithm, □ Chemkin). (b) Grid convergence study showing heat release ($\dot{\omega}_n$).

III.A. Laminar diffusion flame

Figure 1 (a) shows a laminar diffusion flame. The reference variables for the diffusion flame are shown in table 1. Note that M_r, τ_r, T_r, and ρ_r are reference Mach number, reference time, reference temperature, and reference density, respectively. For all simulations, Re is 1000, Pr is 0.7 and μ is equal to $T^{0.7}$. For the unity Lewis number cases, $Le_k = 1$ and the non–unity Lewis numbers are ([6]):

$$Le_{H_2} = 0.3, \quad Le_{O_2} = 1.11, \quad Le_O = 0.7, \quad Le_{OH} = 0.73, \tag{15}$$

$$Le_{H_2O} = 0.83, \quad Le_H = 0.18, \quad Le_{HO_2} = 1.10, \quad Le_{H_2O_2} = 1.12 \tag{16}$$

where $Le_k = \frac{Sc_k}{Pr}$. The initial conditions for the diffusion flame are from Mastorakos et al.:[3]

$$\begin{aligned} Y_{H_2} &= Y^0_{H_2}\zeta(x), \\ Y_{O_2} &= Y^0_{O_2}[1-\zeta(x)], \\ T &= T_O + [T_F - T_O]\,\zeta(x), \\ \alpha(x) &= 0.5\left[1 - \mathrm{erf}\frac{(x-x_c)}{\delta}\right]. \end{aligned} \tag{17}$$

α is the initial conditions for mixture fraction (figure 1 a). Note that δ equal 0.05 which is the thickness of the mixing layer and x_c is the center of the mixing layer where it is equal to π. $Y^0_{H_2}$, $Y^0_{O_2}$, T_O, and T_F are equal to 0.029, 0.233, 4, and 1, respectively. This will yield an equivalence ratio

Table 1. Reference variables.

M_r	τ_r	T_r	ρ_r
0.1	1.48e-4 (sec)	300 (K)	0.8282 (kg/m^3)

(ϕ) of one. The non–dimensional pressure was set to zero. Density was obtained using equation 14. The inlet boundary condition are set to a constant and zero derivative boundary conditions are specified at the outflow.

III.B. Turbulent diffusion flame

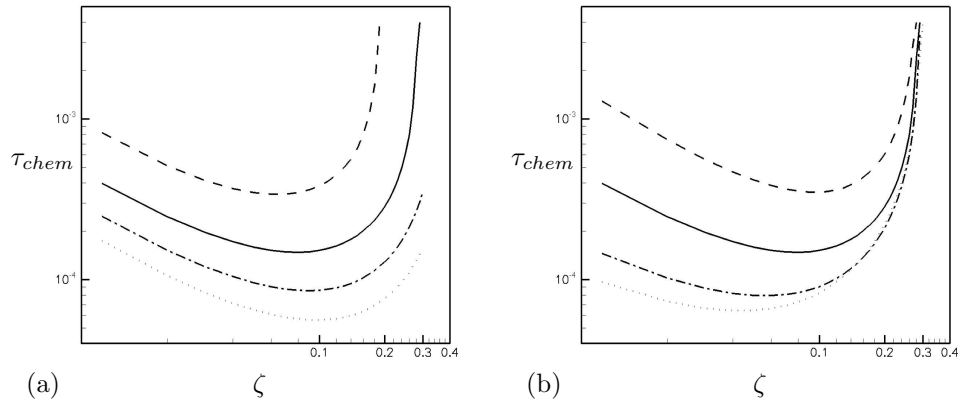

Figure 3. (a) Mixture fraction versus τ_{chem} for varying temperature in kelvin. – – – – $\phi = 1$, $T = 1100$, ——— $\phi = 1$, $T = 1200$, —·— $\phi = 1$, $T = 1300$, **and** ····· $\phi = 1$, $T = 1400$. **(b) Mixture fraction versus τ_{chem} for varying fuel/air ratio,** – – – – $\phi = 1/4$, $T = 1200$, ——— $\phi = 1$, $T = 1200$, —·— $\phi = 4$, $T = 1200$ **and** ····· $\phi = 8$, $T = 1200$.

Three dimensional isotropic turbulence (figure 1 b) is superimposed on the laminar diffusion flame. The initial isotropic turbulence field is prescribed by the three–dimensional kinetic energy spectrum:

$$E(k) = 16\sqrt{\frac{2}{\pi}}\frac{u_0^2}{k_0}\left(\frac{k}{k_0}\right)^4 \exp\left[-2\left(\frac{k}{k_0}\right)^2\right]. \tag{18}$$

The turbulent Reynolds number Re_λ is 50 and k_0 is 5. The computational domain is 2π for x, y, and z. The computational grids for the turbulent diffusion flame are 128 and 256 cubed. All turbulent diffusion flame figures are 128 cubed excect figure 9 which is 256 cubed.

III.C. Validation

The homogeneous mixture problem is used to validate the complex chemistry. Figure 2 (a) is a comparison to Chemkin.[11] Good agreement is observed for the homogeneous mixture problem. A grid convergence study was performed for the laminar diffusion flame. Figure 2 (b) shows results from the grid convergence study. Uniform grids ranging from 64 to 2048 points were used. A grid–converged solution is obtained for a grid of 128 points.

IV. Results

IV.A. Homogeneous mixture problem

Mastorakos et al.[3] used one–step chemistry and the homogeneous mixture problem to obtain τ_{chem} and the mixture fraction most likely to auto–ignite (ζ_{MR}). We obtain ζ_{MR} for the Mueller mechanism (Mueller et al.[2]). The chemical mechanism is a 9 species (H_2, O_2, OH, O, H, H_2O, HO_2, H_2O_2, and N_2), 19 reaction mechanism. Figure 3 (a) shows mixture fraction versus τ_{chem} for initial temperatures that range from 1100 to 1400 Kelvin and figure 3 (b) shows mixture fraction versus τ_{chem} for fuel/air ratios (ϕ) that range from 0.25 to 8. Note in figure 3 that the minimum τ_{chem} corresponds to ζ_{MR}. Figure 3 also shows the effect of fuel/air mixture and temperature on τ_{chem}. As temperature increases, τ_{chem} becomes smaller and ζ_{MR} shifts to the right. As ϕ increases, τ_{chem} becomes smaller and ζ_{MR} shifts to the left. These results illustrate the balance between adequate fuel and high enough temperature for auto–ignition to occur. Table 2 lists the most reactive mixture fraction and corresponding values of the initial temperature, fuel/air ratio and τ_{chem}. Oxidizer temperature of 1200 K (T_0) and ϕ of one is used in the turbulent simulations.

Table 2. Results of homogeneous problem.

T_0	ϕ	ζ_{MR}	τ_{chem}	T_{MR}
1100	1	0.06	$3.4e-4$	1052
1200	1	0.08	$1.48e-4$	1128
1300	1	0.09	$8.5e-5$	1210
1400	1	0.10	$5.6e-5$	1290
1200	1/4	0.1	$3.5e-4$	1110
1200	4	0.06	$8.0e-5$	1146
1200	8	0.04	$6.4e-5$	1164

IV.B. Auto–ignition of diffusion flame

This section discusses auto–ignition of the diffusion flame and its relation to temperature and mixture fraction. The passive scalar and mixture fractions used in the simulations are defined as:

$$\frac{\partial \rho Z}{\partial t} + \frac{\partial \rho Z u_j}{\partial x_j} = \frac{1}{ReSc_Z}\frac{\partial}{\partial x_j}\left(\mu \frac{\partial Z}{\partial x_j}\right), \tag{19}$$

$$\zeta_P = \frac{1}{\phi + 1}\left(\phi \frac{Y_F}{Y_F^0} - \frac{Y_O}{Y_O^0} + 1\right), \tag{20}$$

$$Z_H = W_H\left(\frac{2Y_{H_2}}{W_{H_2}} + \frac{Y_H}{W_H} + \frac{2Y_{H_2O}}{W_{H_2O}} + \frac{Y_{OH}}{W_{OH}} + \frac{Y_{HO_2}}{W_{HO_2}} + \frac{2Y_{H_2O_2}}{W_{H_2O_2}}\right), \tag{21}$$

$$Z_O = W_O\left(\frac{2Y_{O_2}}{W_{O_2}} + \frac{Y_O}{W_O} + \frac{Y_{H_2O}}{W_{H_2O}} + \frac{Y_{OH}}{W_{OH}} + \frac{2Y_{HO_2}}{W_{HO_2}} + \frac{2Y_{H_2O_2}}{W_{H_2O_2}}\right),$$

$$\zeta_B = \frac{\frac{1}{2}Z_H/W_H + \left(Y_{O_2}^0 - Z_O\right)/W_O}{\frac{1}{2}Y_{H_2}^0/W_H + Y_{O_2}^0/W_H}.$$

Here Z denotes the passive scalar variable. ζ_P and ζ_B denote mixture fractions from Poinsot & Veynante[12] and Hilbert & Thevenin,[8] respectively. Note that ζ_B includes all species where ζ_P accounts for only fuel and oxidizer. For the passive scalar equation, Sc_Z was chosen to be 0.7. Figure 4 is scatter plot of the laminar diffusion flame for unity and non–unity Lewis number. If the passive scalar and mixture fraction were equal, one would obtain a straight line. Note that the unity

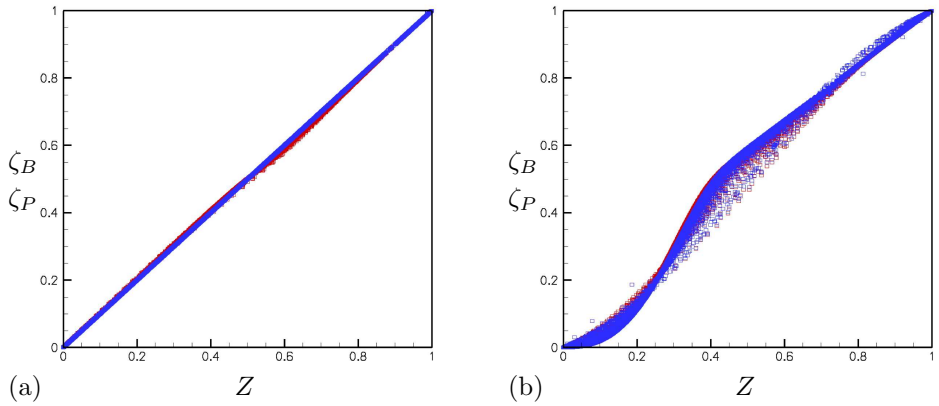

Figure 4. (a) scatter plot of the laminar diffusion flame with unity Lewis number mixture fraction (□ ζ_B and □ ζ_P) versus passive scalar (Z) from a non–dimensional time of zero to 10. (b) scatter plot of the laminar diffusion flame with non–unity Lewis number mixture fraction (□ ζ_B and □ ζ_P) versus passive scalar (Z) from a non–dimensional time of zero to 10.

Lewis number yields a straight line but the non–unity Lewis number does not. These results show that mixture fraction (as defined above) is a conserved scalar for the unity Lewis number but not the non–unity Lewis number. Figure 4 also shows the slight differences between ζ_P and ζ_B, observed well after the formation of products. Therefore, ζ_P is adequate for studying auto–ignition and from now on, $\zeta = \zeta_P$.

Figure 5 (a) illustrates the evolution of ignition for the laminar diffusion flame. Note that ignition occurs in fuel lean, high temperature regions ($\zeta = \zeta_{MR} = 0.08$) and propagates towards the stoichiometric side ($\zeta = 0.5$). Unity Lewis number behaves in a similar manner, but ignition occurs at a later time (figure 5 a). Recall that for unity Lewis number, the mixture fraction is a passive scalar. Therefore, auto–ignition occurs in the same region (ζ_{MR}). On the other hand, for non–unity Lewis number, auto–ignition occur at $\zeta_P = \zeta_B = 0.08$ for the mixture fractions and $Z = 0.13$ for the passive scalar. This result shows that auto–ignition occurs in a 'richer' region for the passive scalar equation than the mixture fraction for non–unity Lewis number.

For the turbulent diffusion flame, figures 6, 7 and 8 show the evolution of T, Y_{HO_2}, and Y_{OH}, respectively. Each contour plot is separated by a unit of time from zero to four. Figure 6 illustrates the effect of auto–ignition on temperature. In figures 7 and 8, note the differences between Y_{HO_2} and Y_{OH}, especially the range of length scales.

Contour plots (in the $x = \pi$ plane) of $\dot{\omega}_n$, T, ζ_2, χ_2, Y_{HO_2}, and $|\omega|$ at a non–dimensional time of 0.9 for the turbulent diffusion flame are shown in figure 9. The contour lines represent the mixture fraction over the range from 0.05 to 0.30. Note that ignition occurs in fuel lean regions (9 a). Echekki and Chen define such ignition sites as kernels. They describe the kernels sites as regions of high–temperature (9 b), fuel–lean mixtures (9 (c)) and low dissipation rates (9 (d)) which is present in figure 9. Note that scalar dissipation is defined as:

$$\chi = \frac{2}{Re}\left(\frac{\partial\zeta}{\partial x_j}\frac{\partial\zeta}{\partial x_j}\right). \tag{22}$$

In the turbulent diffusion flame, there will also be regions with low vorticity (figure 9 e). The ignition sites have low vorticity which allows time for fuel and oxidizer to diffuse together to form essential products for auto–ignition to occur e.g. HO_2. The formation of HO_2 is the precursor to auto–ignition (Im et al.[6]) and is shown in figure 9 (f).

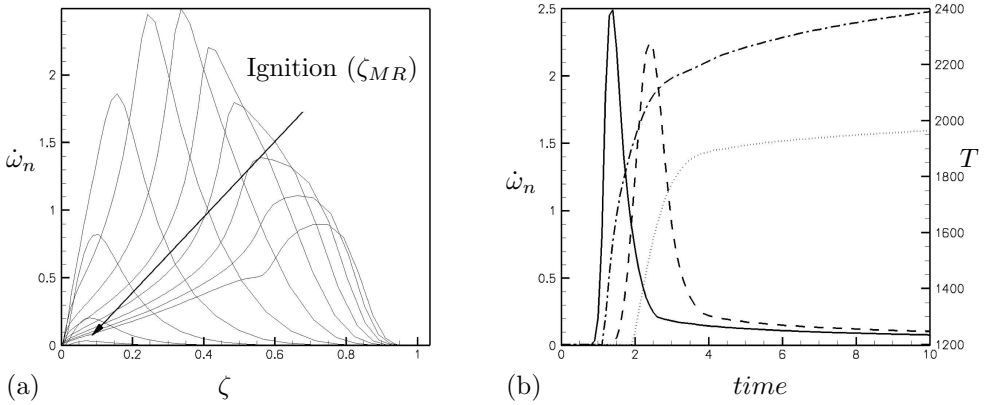

Figure 5. (a) evolution of mixture fraction versus heat release and the location of ignition ζ_{MR}. (b) temporal evolution of maximum heat release and temperature for the laminar diffusion flame. ····· temperature of unity Lewis number, —·— temperature of non–unity Lewis number, – – – – heat release of unity Lewis number, and ——— heat release of non–unity Lewis number.

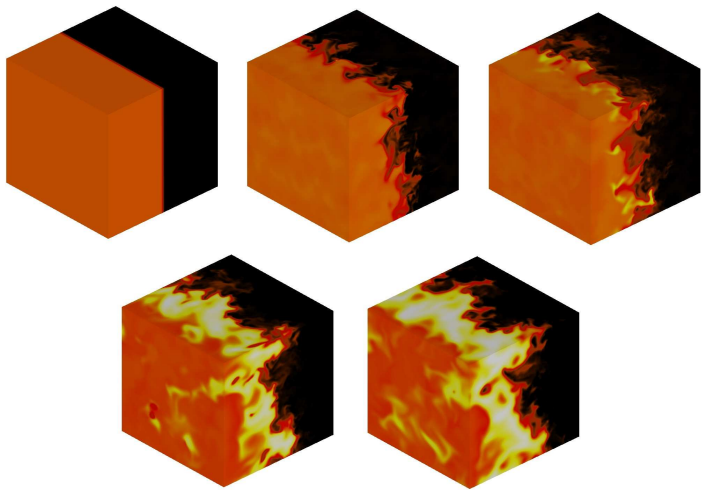

Figure 6. Evolution of temperature from a non–dimensional time of 0 to 4.

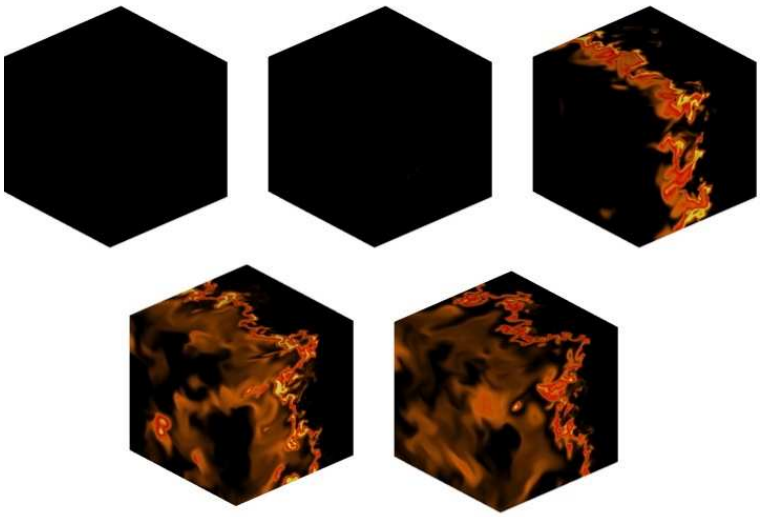

Figure 7. Evolution of Y_{HO_2} from a non–dimensional time of 0 to 4.

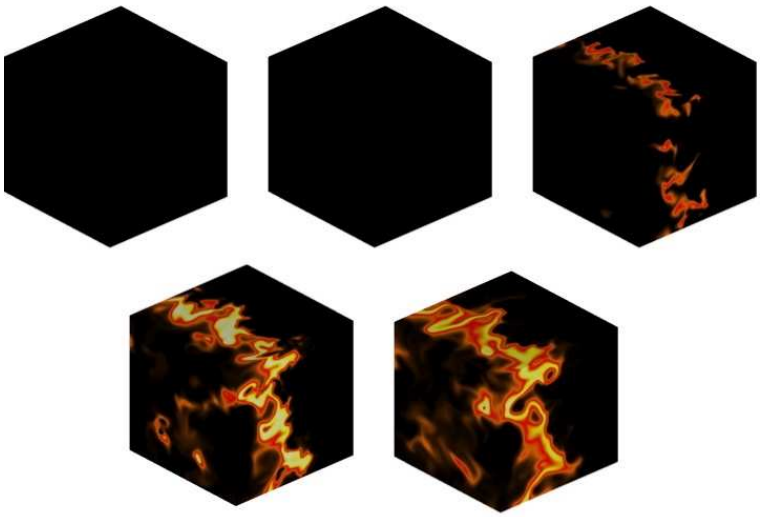

Figure 8. Evolution of Y_{OH} from a non–dimensional time of 0 to 4.

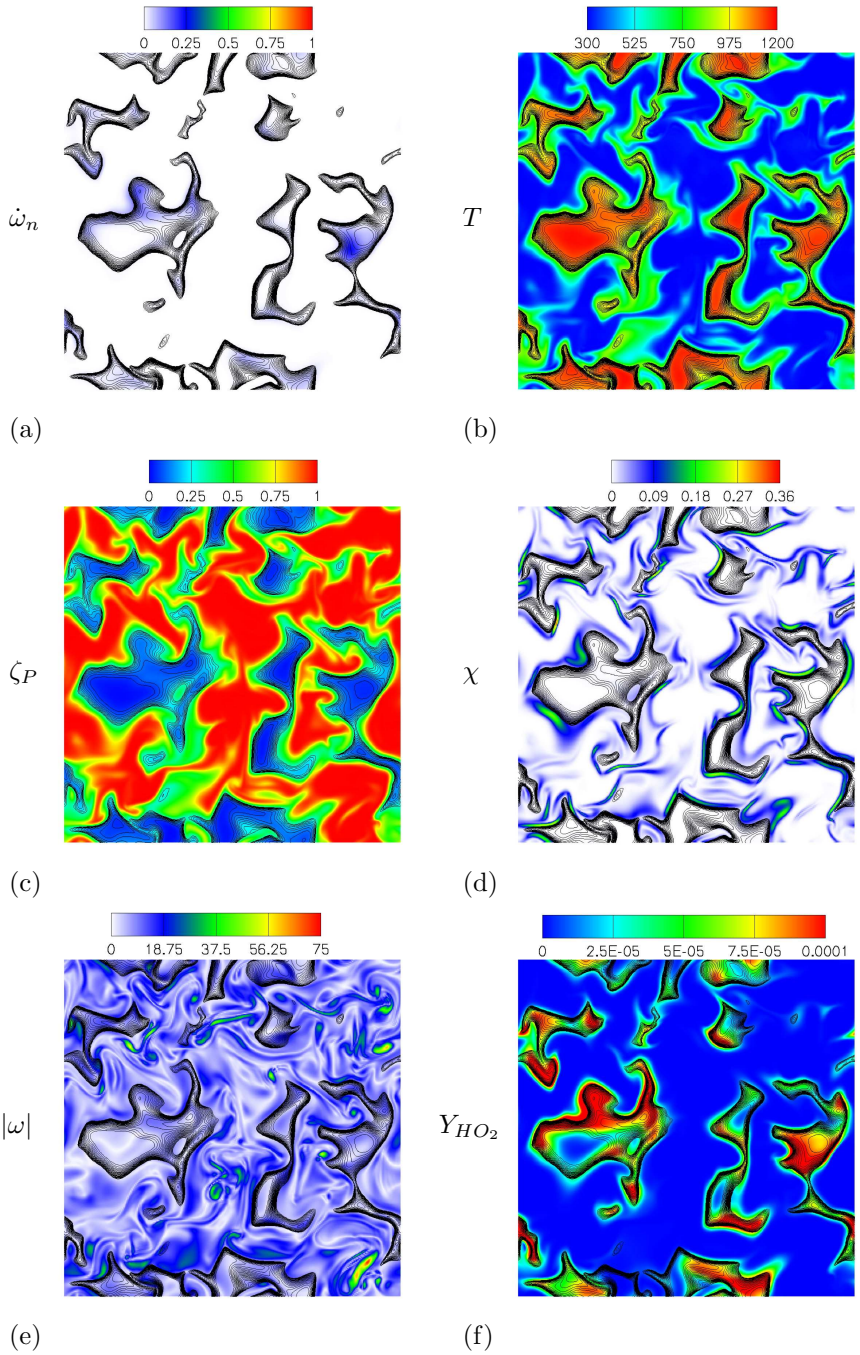

Figure 9. Contour plot of $\dot{\omega}_n$, T, ζ, χ_2, Y_{HO_2}, and $|\omega|$ at a non–dimensional time of 0.9. Contour lines are superimposed for the mixture fraction ζ and range from 0.05 to 0.30.

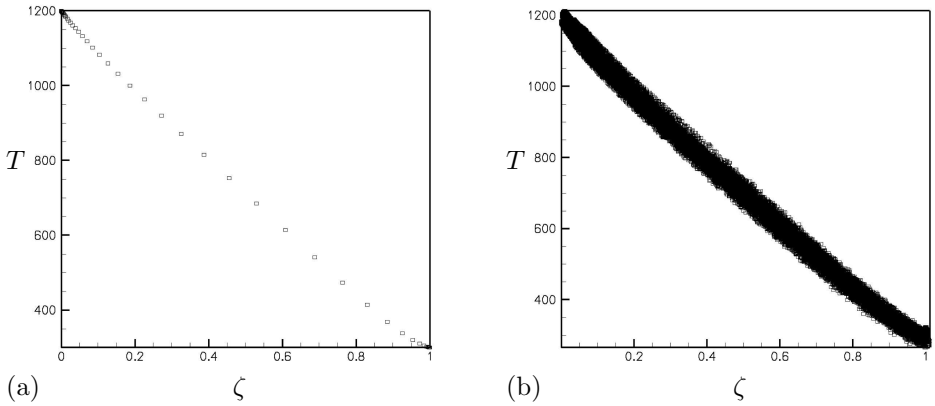

Figure 10. Plot of mixture fraction (ζ) versus Temperature in Kelvin (T) (a) laminar diffusion flame and (b) is the turbulent diffusion flame.

Figure 10 shows the effect of mixing on auto–ignition at ζ_{MR}. Recall from the laminar diffusion flame that auto–ignition occurred at $\zeta = \zeta_{MR} = 0.08$ (figure 5 a). The homogeneous mixture problem predicted the onset of ignition (ζ_{MR}) very well for the laminar diffusion flames. On the other hand, ζ_{MR} does not entirely predict the onset of ignition for the turbulent diffusion flame. This phenomenon is completely due to the turbulent mixing which results in a range of temperatures for a given mixture fraction. For example, if $\zeta = 0.2$, then temperature ranges from 950 K to 1050 K (figure 10 b). Recall from the homogeneous mixture problem, that temperature plays an important role in auto–ignition. Table 2 illustrate that a 100 Kelvin difference changes τ_{chem} by a factor of 2.3. For the turbulence case, this can greatly affect the onset of ignition and location. This is why auto–ignition occurs in a very broad range for ζ_{MR} in the turbulent diffusion flame while the laminar case is at ζ_{MR}.

These results suggest that maybe one should track temperature instead of mixture fraction in predicting auto–ignition and the evolution of ignition. Figure 11 superposes contour lines of temperature which are chosen to range from 950 to 1150 K ($T_{MR} = 1200 - \zeta_{MR}\,[1200 - 300]$). Interestingly, maximum heat release follows T_{MR} at every instant of time in figure 11. This figure shows that the onset of ignition occurs at ζ_{MR} and T_{MR}. As ignition continues, ζ_{MR} is in the very fuel lean region and does not follow the path of ignition. T_{MR} on the other hand, follows the path of ignition at each instance in time. This suggests that T_{MR} instead of ζ_{MR} might be better choice in predicting the evolution of auto–ignition.

IV.C. The effect of Lewis number

Figure 5 (a) shows the profiles of maximum heat release and temperature versus time for the laminar diffusion flame. Note that ignition occurs at a non–dimensional time of around 1.6 for the one dimensional diffusion flame with unity Lewis number while ignition occurs around 1 for the non–unity Lewis number. The temperature difference between the unity Lewis number and non–unity Lewis number is 450 K. The fastest ignition time was obtained for the non–unity Lewis number turbulent diffusion flame. The first signs of auto–ignition starts around 1.6, 1.0, 1.4 and 0.9 (non–dimensional time) for the laminar unity Lewis number, laminar non–unity Lewis number, turbulent unity Lewis number and turbulent non–unity Lewis number, respectively. These results shows that differential diffusion plays an important in the auto–ignition of the diffusion flame. The difference

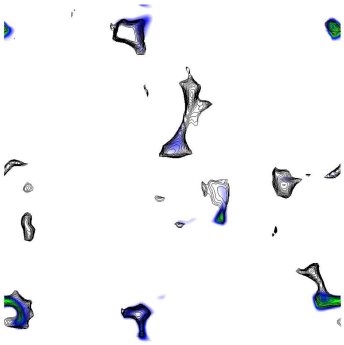

ζ at time = 1.8

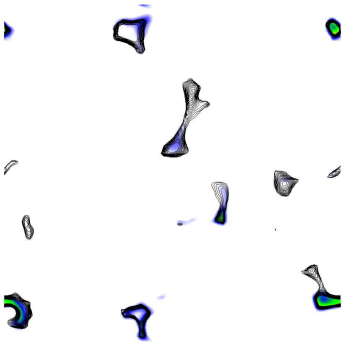

T at time = 1.8

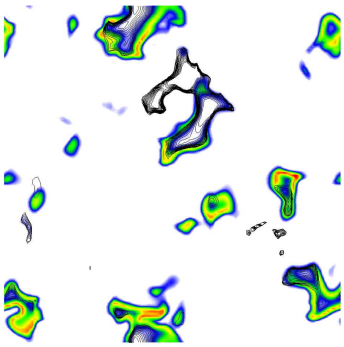

ζ at time = 2.2

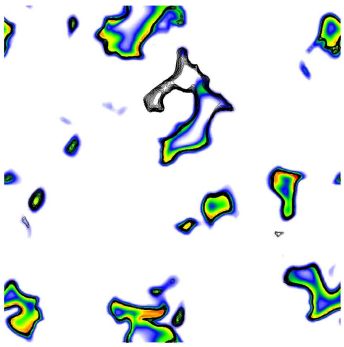

T at time = 2.2

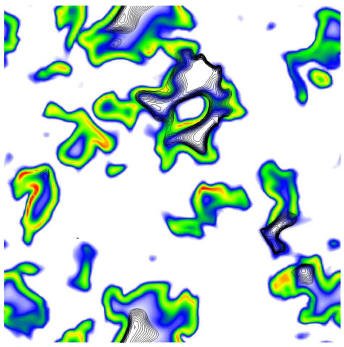

ζ at time = 2.6

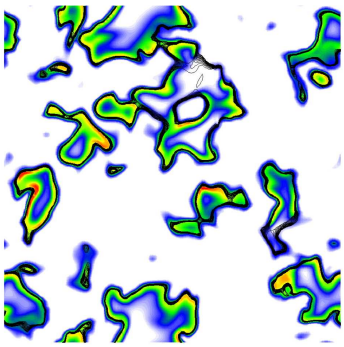

T at time = 2.6

Figure 11. Contour lines of mixture fraction (0.05 to 0.3) and temperature (950 to 1150 K) superposed on shaded contours of reaction rate at different instants of time.

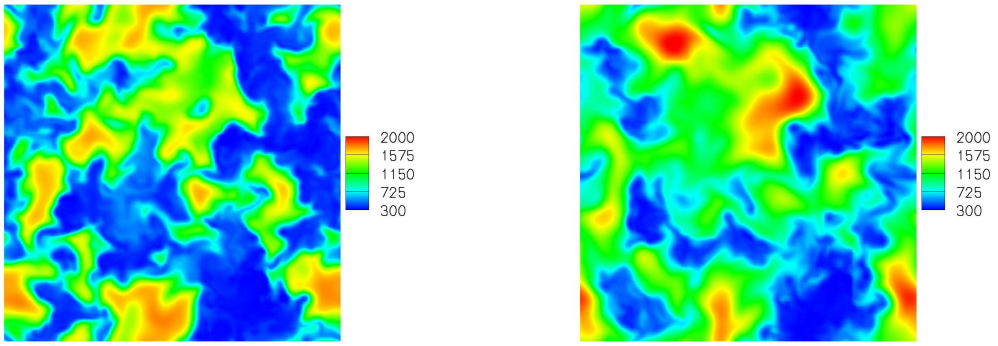

(a) (b)

Figure 12. Comparison of temperature for (a) unity Lewis number and (b) non–unity Lewis number at a non–dimensional time of 3.

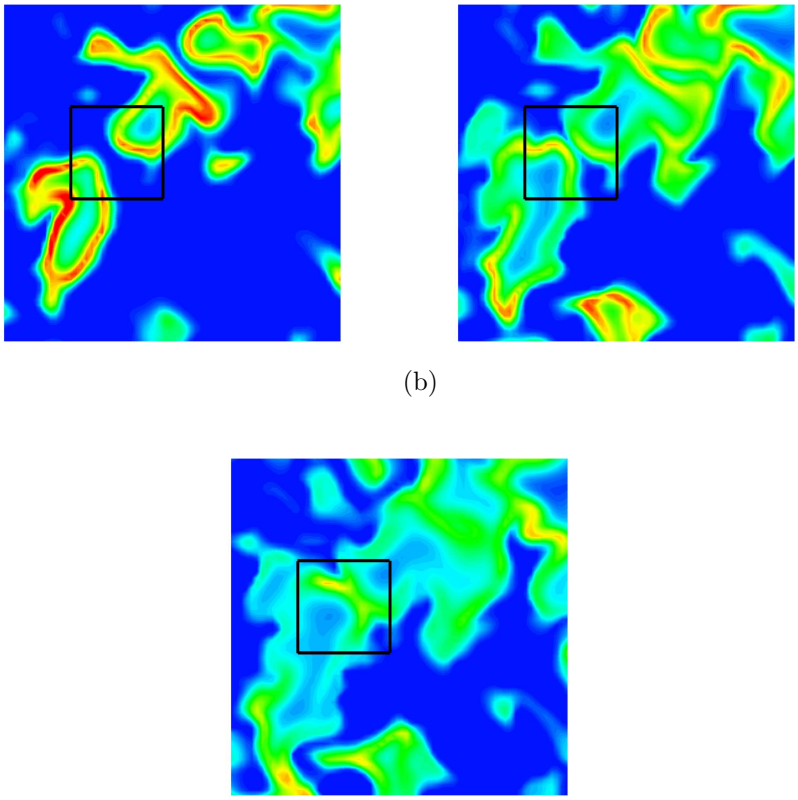

(a) (b)

(c)

Figure 13. Contour plots of $\dot{\omega}_n$ showing time evolution of flame fronts. (a) time = 2.6, (b) time = 2.9, and (c) time = 3.2.

between the turbulent unity Lewis number and non–unity Lewis number is further demonstrated in figure 12. The comparison between temperature in figure 12 shows that the two cases are complete different, i.e. viscous diffusion is important even in the turbulent regime.

IV.D. Evolution of ignition fronts

It is generally felt (e.g. Hilbert & Thevenin[8] and Mahalingam et al.[4]) that the main difference between three dimensional and two dimensional turbulent simulation is that two dimensional turbulence lacks vortex stretching and high dissipation rates. Our results suggest that three-dimensional simulations do matter in the collision of flame front and that dimensionality affects the results at a more fundamental level. Mastorakos et al[3] performed two-dimensional simulations using one–step chemistry. They found that fronts propagate outward and collapse at the very lean or rich sides due to extinction, or after collisions with separate similar fronts originating from other ignition sites.[3] Our results show that when flame fronts collide; they can either increase in intensity, combine without any appreciable change in intensity, or extinguish. In most cases, the flame fronts combine together (figure 13). This phenomenon is due to the extra dimension. In two–dimensional simulations when flame fronts collide, there is no extra dimension for products to travel which 'chokes' the flow. In the three-dimensional simulation, products can migrate to the extra dimension which allows the flame fronts to combine together.

V. Summary

The paper uses direct numerical simulation to study auto–ignition of a hydrogen/air turbulent diffusion flame. A detailed chemical mechanism due to Mueller et al[2] is used. Simulations of three dimensional turbulent diffusion flames were performed. Isotropic turbulence is superimposed on an unstrained diffusion flame where diluted H_2 at ambient temperature interacts with hot air. Both, unity and non–unity Lewis number are studied. The results are contrasted to the homogeneous mixture problem and a laminar diffusion flames. Results show that auto–ignition occurs in fuel lean, low vorticity, and high temperature regions with low scalar dissipation around 'most reactive' mixture fraction, ζ_{MR}. For the laminar case, auto-ignition occurs at ζ_{MR} while the turbulent case auto–ignites occurs in a very broad range of ζ_{MR}. Simulation also study the effects of three-dimensionality of the turbulent diffusion flame. Two–dimensional simulations show that when flame fronts collide, extinction occurs (Mastorakos et al.[3]). Our results show that when flame front collide; they can either increase in intensity, combine together or go extinct which is due to the extra dimension. Three dimensional simulations are essential to turbulent diffusion flames and in particular, the collision of flame fronts. Ignition kernels are related to the most reactive mixture fraction, but the most reactive fraction cannot completely predict the onset of ignition because ignition occurs in a broad range of ζ_{MR}. We also show that the passive scalar equation does not agree with non–unity Lewis number mixture fraction and that viscous diffusion is important even in the turbulent regime.

VI. Acknowledgments

This work was supported by the AFOSR under grant FA9550–04–1–0341 and by the Doctoral Dissertation fellowship awarded by the Graduate School at the University of Minnesota. Computing resources were provided by the Minnesota Supercomputing Institute, the San Diego Super–computing Center and the National Center for Supercomputing Applications.

References

[1] J. Doom, Y. Hou, K. Mahesh, A numerical method for DNS/LES of turbulent reacting flows. *J. Comput. Phys.* **226** (2007) 1136–1151.

[2]M.A. Mueller, T.J. Kim, R.A. Yetter, F.L. Dryer, Flow Reactor Studies and Kinetic Modeling of the H2/O2 Reaction. *Int. J. Chem. Kinet.* **31** (1999) 113–125.

[3]E. Mastorakos, T. A. Baritaud, T. J. Poinsot, Numerical simulations of autoignition in turbulent mixing flows. *Comb. Flame* **109** (1997) 198–223.

[4]S. Mahalingam, J.H. Chen, L. Vervisch, Finite–rate chemistry and transient effects in direct numerical simulations of turbulent nonpremixed flames. *Comb. Flame* **102** (1995) 285–297.

[5]C.J. Montgomery, G. Kosaly, J.J. Riley, Direct numerical solution of turbulent non–premixed combustion with multistep hydrogen–oxygen kinetics. *Comb. Flame* **109** (1997) 113–144.

[6]H. G. Im, J. H. Chen, C. K. Law, Ignition of hydrogen mixing layer in turbulent turbulent flows. *27th Symp. (Int.) on Comb.* (1998) 1047–1056.

[7]T. Echekki, J.H. Chen, Direct numerical simulation of auto–ignition in non–homogeneous hydrogen–air mixtures. *Comb. Flame* **134** (2003) 169–191.

[8]R. Hilbert, D. Thevenin, Autoignition of turbulent non–premixed flames investigated using direct numerical simulations. *Comb. Flame* **128** (2002) 22–37.

[9]R. Hilbert, D. Thevenin, Influence of differential diffusion on maximum flame temperature in turbulent nonpremixed hydrogen/air flames. *Comb. Flame* **138** (2004) 175–187.

[10]Thompson, P.A., Compressible-fluid Dynamics. New York: McGraw-Hill, 1972.

[11]R. J. Kee, F. M. Rupley, J. A. Miller, M. E. Coltrin, J. F. Grcar, E. Meeks, H. K. Moffat, A. E. Lutz, G. Dixon-Lewis, M. D. Smooke, J. Warnatz, G. H. Evans, R. S. Larson, R. E. Mitchell, L. R. Petzold, W. C. Reynolds, M. Caracotsios, W. E. Stewart, P. Glarborg, C. Wang, C. L. McLellan, O. Adigun, W. G. Houf, C. P. Chou, S. F. Miller, P. Ho, P. D. Young, D. J. Young, D. W. Hodgson, M. V. Petrova, and K. V. Puduppakkam, CHEMKIN Release 4.1, Reaction Design, San Diego, CA (2006)

[12]Poinsot, T., & Veynante, D., 2005, Theoretical and Numerical Combustion. *Edwards*.